Artificial Intelligence in Nuclear Medicine Physics and Imaging

Konstantinos Papachristou[2]
Emmanouil Panagiotidis[1] **MD, PhD**
Anna Makridou[2] **MSc, PhD**
Theodoros Kalathas[1] **MD, Msc**
Vasilis Masganis[2]
Anna Paschali[1] **MD, PhD**
Maria Aliberti[2] **Msc**
Vasiliki Chatzipavlidou[1] **MD, Msc**

1.Nuclear Medicine Department, Cancer Hospital of Thessaloniki "Theagenio"
2.Medical Physics Department, Cancer Hospital of Thessaloniki "Theagenio"

Keywords: Artificial Intelligence
- Imaging Physics
- Image reconstruction
- Low dose Imaging

Corresponding authors:
Anna Makridou MSc, PhD, MPE, RPE,
Medical Physics Department,
Cancer Hospital Thessaloniki
Theagenio, 2 Al Symeonidisstr,
54007 Thessaloniki, Greece
anna.makridou@gmail.com

Received:
13 March 2023
Accepted revised:
24 March 2023

Abstract
No one can deny the significant impact of artificial intelligence (AI) on everyday life, especially in the health sector where it has emerged as a crucial and beneficial tool in Nuclear Medicine (NM) and molecular imaging. The objective of this review is to provide a summary of the various applications of AI in single-photon emission computed tomography (SPECT) and positron emission tomography (PET), with or without anatomical information (CT or magnetic resonance imaging (MRI)). This review analyzes subsets of AI, such as machine learning (ML) and Deep Learning (DL), and elaborates on their applications in NM imaging (NMI) physics, including the generation of attenuation maps, estimation of scattered events, depth of interaction (DOI), time of flight (TOF), NM image reconstruction (optimization of the reconstruction algorithm), and low dose imaging.

Hell J Nucl Med 2023; 26(1): 57-65 *Published online: 28 April 2023*

Introduction

The term AI was coined in 1955 to broadly describe the use of computer algorithms to perform tasks associated with human intelligence, such as learning or problem-solving [1, 2]. In recent years, AI has become increasingly prevalent in radiology, driven in part by the fact that since 2015, visual recognition using AI has had a lower error rate than that of humans [2, 3]. This has been made possible by the rapid progress in AI technology, which has been enabled by increasing computational power, novel algorithms, and available data. The healthcare industry has not been immune to these advances, with a growing amount of data being generated by novel imaging procedures and diagnostic imaging procedures, enabling opportunities for personalized and precision medicine. However, this wealth of information is overwhelming for physicians, and sophisticated AI algorithms are needed to exploit it. Specifically in medical imaging, and particularly in Nuclear Medicine imaging (NMI), AI can be used to improve the entire imaging pipeline, from improving image quality to increasing acquisition speed and lowering costs during image acquisition and reconstruction. Additionally, AI can be utilized for image denoising, registration, and translation between different modalities. Finally, many AI applications for medical image analysis are being developed, including abnormality detection, segmentation, and computer-aided diagnosis [4].

Terminology

This section presents several definitions of machine learning and related concepts in order to fully understand their structure and usage, with a focus on their applications in NM, specifically in positron emission tomography (PET) and single-photon emission computed tomography (SPECT) imaging, which will be discussed in upcoming sections. Starting with the definitions provided by Tang et al. (2018) and Lundervold et al. (2019), a subtype of AI known as "machine learning" (ML) employs algorithms through data analysis without explicit programming [1, 5]. After learning from human-defined teaching cases, ML is frequently associated with resolving logic-related issues. Machine learning, being a subset of AI, is not a single algorithm but rather analyzes a set of training data to build a model that carries associations between the variables that are important for a specific outcome. Data extraction and filtration typically require handcrafted features, requiring more human involvement [6]. Regarding the subsets of ML, the first and most crucial is deep learning (DL). Chartrand, Castiglioni et al. (2017, 2021) emphasize that DL

automates many parts of input extraction, enabling less human intervention [6-8]. Tang et al. (2018) describe DL as adding several processing layers (depth) to detect complex features in an image [1]. Schulz et al. (2020) suggest that logistic regressions can be combined into hierarchies with neural networks, allowing for intricate interactions between input variables to improve model performance [9]. In DL, the model may accept raw data, such as images, rather than summary features that rely on human interaction. The human intervention in DL is far more limited in contrast to ML [6-8]. Deep learning consists of three subfields: Artificial neural networks (ANN), convolutional neural networks (CNN) and generative adversarial networks (GAN). Artificial neural networks have linked nodes with weighted paths, where each node has parent nodes that it responds to, an activation function, a firing threshold, and an output value. Artificial neural networks and their communication are comparable to that of neurons [7, 9]. While an ANN typically receives feature data as input, a CNN instead, uses a convolutional process to extract features from the image itself [1]. Convolutional neural networks systematically traverse an image after applying a neural-network layer to a specific area of the image. By alternating convolutional layers with pooling layers, CNN sample and condense features, which results in lower computational requirements [7, 9]. Finally, GAN consist of two networks, a generator and a discriminator, which play a zero-sum game to reduce the difference between fake and genuine inputs. Generators produce fictitious input data to reduce this difference, while the discriminator sorts the genuine and fake inputs to maximize efficiency [7]. To better comprehend the structure and chain of command, all of this information is summarized in Figure 1.

According to Uribe et al. (2019), big data, or at least, large datasets for training, the availability of improved hardware, and the fact that ML is an effective tool for analyzing extracted features in radiomics have all led to increased usage of ML in recent years [10]. The field of AI known as ML is utmost significance. For a very long time, traditional ML techniques like naive Bayes, support vector machines, and random forests were used extensively in the medical field. Positron emission tomography (PET) [15], single-photon emission computed tomography (SPECT) [11, 12], prognosis PET [13], SPECT [14], lesion classification PET [15], SPECT [16, 17], and imaging physics are some of the applications of ML in NM imaging [18]. Artificial neural networks, GAN, and other DL technologies have advanced quickly in recent years and have occasionally outperformed traditional ML. The use of DL in NM includes the diagnosis of disease using PET [19], SPECT [20,21], imaging physics using PET [22], SPECT [23], image reconstruction using (PET [24],SPECT [25]) image denoising (PET [26, 27], SPECT [28]), image segmentation (PET [29], SPECT [30]) and image classification (PET [31], SPECT [32]). A similar approach is presented in [2, 33-35], referring to the detection and classification of diseases or lesions, automated image segmentation, pre-analysis, and quantitation, the extraction of radiomic features from image data, image reconstruction, case triage and reporting prioritization, research and data mining, and natural language processing as examples of specific ML capabilities. In summary, the aim of ML and its subsets is to achieve optimal replication while ensuring the best possible fit to the observed data, leading to improved predictive performance [36].

Imaging physics – Data correction

This section provides a thorough analysis of the implementation of AI in imaging physics-data correction, particularly in the generation of attenuation maps, correction of scatter events, and detection of photon position. Attenuation maps and scatter correction are currently the focal point of intense research in nuclear medicine for PET and SPECT imaging, with several AI groups contributing to the field [37].

Attenuation correction (AC)

Obtaining high-resolution PET images is challenging due to photon attenuation, which is the loss of photon flux intensity through a medium. One example of an unavoidable factor that causes attenuation is the photon's interaction with body tissue before detection. For larger samples of people, this can lead to image distortion, artifact formation, and loss of resolution. Attenuation correction (AC) is one method used to correct attenuation on an individual basis, which takes place during the data's image processing stage after it has been collected. However, the lack of a direct measurement of photon attenuation makes it difficult to obtain accurate attenuation maps for PET/MR scans or PET imaging alone [11]. The majority of suggested AC methods are based on the broader image-to-image translation field of DL, which is a general AI task [38]. These advancements aim to eliminate the need for ana-

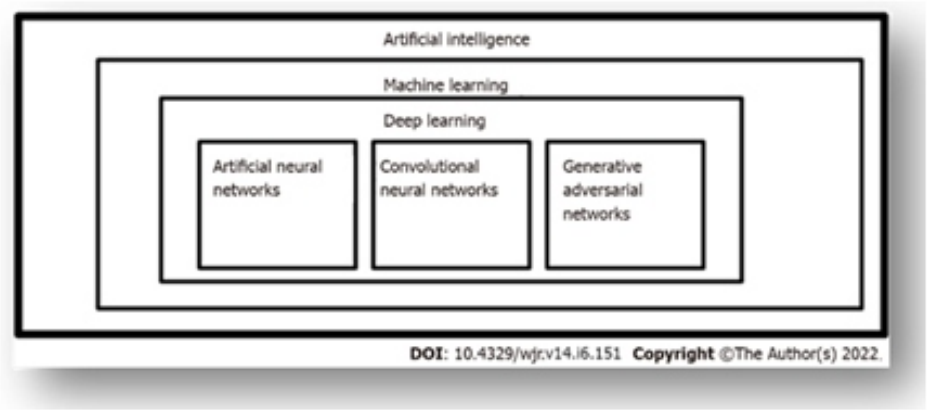

Figure 1. AI subfields.

tomical image data by directly producing AC images from non-AC PET data [39], to produce CT equivalent-based AC maps from MR images in multimodality PET/MR [40], and to improve the attenuation maps produced by maximum likelihood reconstruction of activity and attenuation (MLAA) approaches [41]. To automate the AC process for PET images without input from a different anatomical image, such as a CT scan, Liu et al. (2018) recently developed a deep ML algorithm. Initially, fluorine-18-fluorodeoxyglucose (^{18}F-FDG) PET/CT datasets were used to train the model. As a result, it was possible to create and refine continuously valued "pseudo-CT" images solely using the uncorrected ^{18}F-FDG images that served as the basis for the attenuation map. Deep AC's output, an AC ^{18}F-FDG image, was found to be quantitatively accurate with typical errors under 1% [42]. Similarly, Ladefoged et al. (2019) implemented a deep unsupervised transfer learning encoder-decoder method for PET/ MR-AC intended for kids with possible brain tumors [43]. Hwang et al. (2019) used a modified U-Net to generate the attenuation maps for whole-body PET/MRI [41], where U-Net is a specialized convolutional network architecture for biomedical image segmentation [44]. High-resolution features can be combined in the output layers thanks to the contracting path enhancement provided by U-Net [45]. According to Cheng et al. (2021), GAN is more widely used in attenuation map generation and forecast than other DL [45]. Shi et al. (2020) designed a GAN to produce the SPECT attenuation map obliquely from the emission data. The SPECT images from the scatter window and photopeak window served as their inputs, and this method can successfully uncover any attenuation-related hidden information in the emission data [46]. Cycle-consistency networks known as Cycle-GAN are a subset of GAN. A Cycle-GAN is composed of two mirror-symmetric GAN and has been used for whole-body PET AC according to Dong et al. (2019, 2020) [47, 39]. In [48], GAN is referred to as a specific type of GAN that aims to perform image translation when dealing with unpaired data, as is done for MRI-based PET attenuation correction. Similar work is done by Armanious et al. (2020) [49], who developed and assessed a conditional GAN method for the AC of ^{18}F-FDG PET images of the brain. Looking to the future [50, 51], residual encoder-decoder networks can produce attenuation and scatter-corrected PET images without the use of attenuation maps, starting from the non-corrected images.

Scatter correction (SC)

A gamma photon may experience Compton or Rayleigh scattering as it travels through a scintillation crystal before being absorbed in a different detector block or pixel through photoelectric absorption. Since no optical photons are produced, Rayleigh scattering, an elastic process without energy transfer, is essentially undetectable. On the other hand, the inelastic Compton interactions reduce the amount of energy available for subsequent photoelectric absorption by converting a portion of the gamma energy into scintillation light proportional to the scattering angle. These Compton scattered events are simple to observe for interactions between different crystals or pixels, but it is difficult to identify the first gamma interaction, which can degrade images in PET or SPECT due to incorrectly assigned LOR or counts. As a result, they are frequently thrown away, which reduces their sensitivity [4]. When it comes to SC, the scatter sinograms could be created using the emission and attenuation raw data from PET or SPECT imaging [36, 24], or they could be created directly using SC images (typically combined with AC) using non-corrected PET images as the network's input data [50]. In order to teach their CNN to replicate the scatter distributions of 57 (training) bed positions, Berker et al. (2018) used measured PET emission data and attenuation correction factors as inputs. They then reconstructed PET images using reference and estimated scatter distributions for SC, using the model to forecast scatter estimates for the 14 remaining (validation) bed positions. In the same paper, it is also mentioned that the application of AI technology in particular regions (such as the brain and lungs) has better SC when compared to whole-body imaging [52]. Finally, two CNN were suggested by Qian et al. (2017) to calculate the SC for PET. The convolutional layer and the fully connected layer of the first network, which only had six layers overall, were used to predict multiple scatter profiles from a single scatter profile. The total scattering distribution (both single and multiple scattering) was directly derived from the emission and attenuation sinograms using the second network. In this instance, the network structure remained the same. As a training label, a scattering Monte Carlo simulation was used [53].

Photon position detection – Depth of interaction (DOI)

The lack of DOI decoding in PET can result in incorrect line-of-response (LOR) assignment for coincident non-perpendicular events, leading to lower accuracy in image reconstruction. As an alternative, a linear method based on scintillation light sharing through a common light guide on the front surface of the crystal was developed for continuous DOI estimation [54]. Later, a neural network estimator was used to enhance the linear method. The SiPM array's measured energies are used as input features to forecast a continuous DOI position. Compared to the linear approach, the dense neural network and CNN performed similarly, but the accuracy improved by 12% to 26%. The crystal array's uniformity was also significantly improved [54]. Michaud et al. (2015) also created a neural network to determine the LOR in PET for triple coincidences, where one 511keV photoelectric event occurs simultaneously with two additional singles S1 and S2 (where S is the position of the photon's position detection), whose combined energies are also 511keV. Analytically determining which single lies on the LOR under ideal conditions is frequently possible by considering the relationship between the scattering angle and energy deposit. However, these analytical techniques suffer from low energy resolution and positioning accuracy. The DL approach seeks to address these limitations by naturally accounting for them with realistic training data. Regarding PET detectors, their primary goal is to stop as many of the 511keV gamma rays as possible and produce output signals that can be detected, saved, and analyzed [56]. Monolithic detectors are a distinct category of detectors that provide easier access to DOI data and are not limited by pixel size for spatial resolution. Early studies have demonstrated that neural networks can provide superior spatial resolution with good uniformity and can predict the

location of the impinging object for oblique incidences without the need to correct for DOI [57-59]. Later works added DOI as an additional output, enabling 3D positioning [60-62].

Time of flight (TOF)

The positron annihilation position can be determined more precisely along the LOR in time-of-flight (TOF) PET, which utilizes interaction timing data. By incorporating this data during image reconstruction, the quality of the scan can be significantly improved [4]. In a study conducted by Berg and Cherry, it was demonstrated that CNN are capable of accurately predicting the TOF difference from the detector signals themselves [63]. In order to predict the TOF difference between two detectors, the study utilized the outputs of two opposing detector pixels, which were digitalized using 100 ps binning and then stacked side by side. Since the crucial timing information is primarily present in the first few arriving scintillation photons, only the signals' brief rising edges were used. This method resulted in a 23% increase in timing resolution compared to constant fraction discrimination and a 20% increase compared to leading edge detection, demonstrating promising results.

Image reconstruction

Artificial intelligence technology has been utilized for nuclear medicine image reconstruction, particularly in PET reconstruction [64]. While AI can help address important reconstruction issues, such as the transformation between the sinogram and image domains or the displacement of regularization in conventional algorithms, it cannot provide a complete solution to the inverse problem. In science, an inverse problem refers to the process of determining the causal factors that produced a set of observations. Although AI has made it possible to improve imaging quality without excessive investments in hardware [45], it is not a panacea for all imaging challenges. Visvikis et al. (2022) have highlighted a fundamental paradigm shift with the inclusion of AI in the reconstruction process. Currently, measured data are mapped to an estimate of the final image by training a reconstruction operator with sufficiently varied and diverse data to account for all conceivable imaging possibilities [36]. In direct reconstruction, training occurs between the raw data (represented by sinograms or projections) and the reconstructed images [65]. Newer methods, such as using GAN that were originally proposed for image-to-image translation [66], make direct AI reconstruction computationally efficient after training is completed. This approach can avoid the inaccurate assumption modeling inherent in conventional methods [64]. One of the best examples of direct DL reconstruction is AUTOMAP (automated transform by manifold approximation) for DeepPET [65]. AUTOMAP suggests a generalized data-driven approach to inverse problems by learning a mapping from sensor-domain to image-domain data, which implicitly learns a low-dimensional joint manifold of the data from both domains during training. The AUTOMAP authors emphasize that it applies to generalized reconstruction issues and also provide an analysis of PET data. In 2018, Zhu et al. reported that using manifold approximation automatic transformation, reconstruction can be re-encoded as a data-driven supervised learning task [67]. The network includes a CAE structure (convolutional autoencoder) with three completely connected layers to improve artifact reduction and reconstruction accuracy for sinogram data from noisy and under-sampled acquisitions. When Zhu et al. (2018) applied AUTOMAP to ^{18}F-FDG PET data, they produced images that were comparable to those created using conventional reconstruction techniques.

Another innovative idea was presented by Häggström et al.

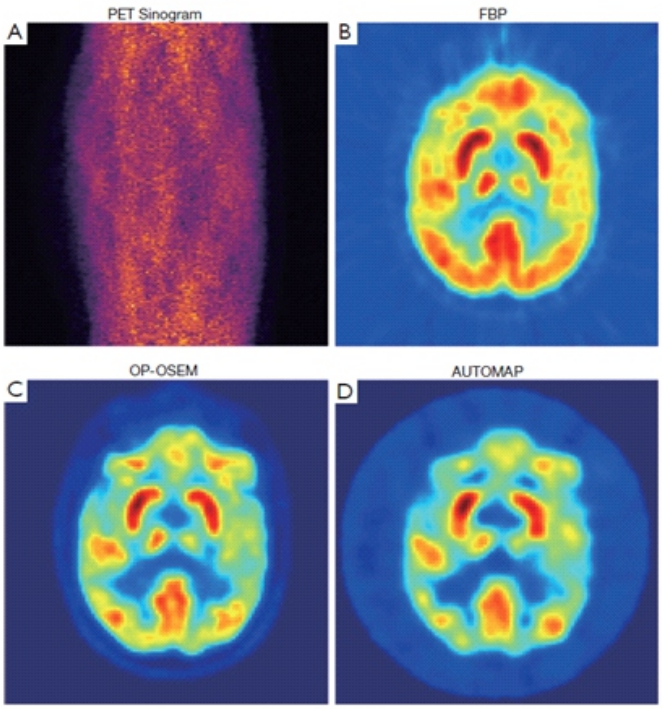

Figure 2. Reconstruction results using the traditional algorithm and Zhu et al.'s method. Human ^{18}F-FDG PET sinogram data (A) was reconstructed using (B) FBP, (C) OP-OSEM, and (D) AUTOMAP. Compared with FBP, AI results are significantly improved and can generate results that are visually similar to OP-OSEM algorithms.

(2019) who developed a convolutional encoder-decoder network called Deep-PET that uses sinogram data as input to create quantitative PET images. Based on metrics such as relative root mean squared error (lower by 53% and 11%, respectively), structural similarity index (higher by 11% and 1%, respectively), and peak signal-to-noise ratio, DeepPET was found to produce images of higher quality than the filtered back projection and OSEM methods (higher by 3.8 and 1.1 dB, respectively). DeepPET also demonstrated a decrease in computational cost for image reconstruction by producing images 3 and 108 times faster than the filtered back projection and OSEM methods, respectively [65]. Going deeper into the DL subsets, Yang et al. (2018) proposed a patch-based image enhancement scheme using a multilayer perception (MLP) ANN model with backpropagation to improve the MAP (maximum a posteriori) reconstructed PET images. The MLP model was trained using 28 image patches that were reconstructed with the MAP algorithm. The MLP method was able to produce images with less noise than the MAP reconstruction algorithm, resulting in a smaller unachievable region [68]. For CNN, Hong et al. (2018) improved the image resolution and noise properties of PET scanners with large pixelated crystals by using a deep residual convolutional neural network (CNN) [69]. Kim et al. (2018) demonstrated that iterative PET reconstruction using a denoising CNN with local linear fitting improved image quality and was resistant to noise-level differences [70]. Another CNN approach is from Liu et al. (2019) who created an image reconstruction algorithm using ML neural networks, consisting of three modified U-Nets (3UNet), to increase the signal-to-noise ratio of PET images obtained from multimodal PET/MR image data without the need for a high-dose PET image. The reconstructed PET image from the 3U-Net model using PET/MR data had a better signal-to-noise ratio compared to those using PET input data alone or PET/MR in a 1U-Net model [71]. Lastly, ResNet, a network architecture based on appending numerous residual blocks one after the other instead of using an encoder-decoder style network with symmetrical skip connections, has potential in image reconstruction. ResNet was modified and applied to denoising PET images in [72]. A significant analysis of the usage of AI in Image reconstruction is seen in Figure 2 [45].

Low dose imaging

The use of radioactive tracers in PET imaging has raised concerns [73] due to the potential risk of developing cancer from high levels of radiation exposure. Therefore, it is preferred to lower the dose of radioactive tracer administered to patients in order to reduce radiation exposure [74]. Especially in children and young adults undergoing repeated scans, dosimetry and dose reduction are an issue [75]. A reduction in the use of radiotracers has been made in an effort to lessen this potential risk in PET imaging. Due to the inherent noise in low-dose PET images, it is challenging to derive qualitative and/or quantitative conclusions from the data [11]. In addition, lowering the dose causes a low signal-to-noise ratio (SNR) and information loss, both of which have a significant impact on clinical diagnosis. Furthermore, low-dose PET image reconstruction presents a challenging problem for iterative reconstruction algorithms due to its poor conditioning [73]. In order to resolve this, efforts have been made to create ML techniques that would permit PET/MR imaging with fewer radiotracers while maintaining the diagnostic quality of the image. The use of ML algorithms to tackle this problem simulates a low dose using a portion (roughly 1% to 25%) of PET data that was collected from a full-dose image. Using only the low-dosage data as input, the ML method then forecasts the images of a full dose [11]. In [73],

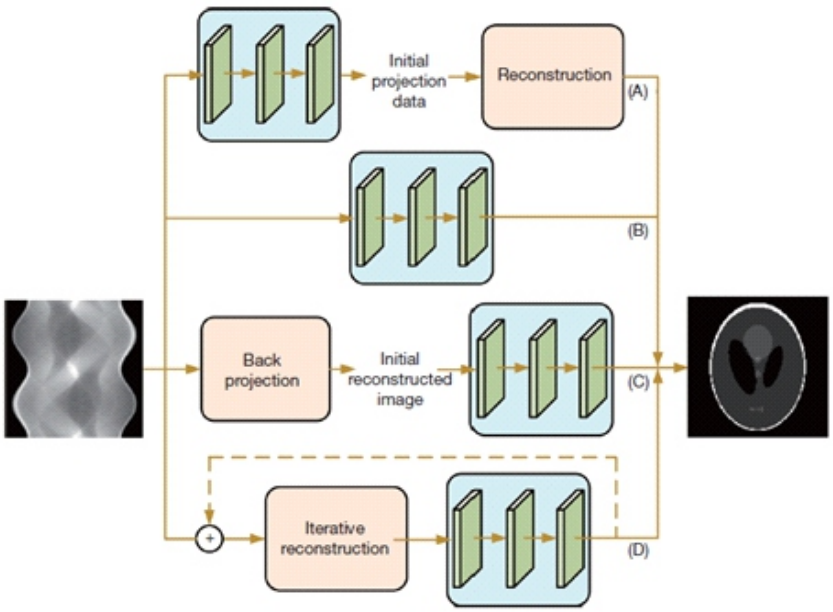

Figure 3. Image reconstruction technique for static nuclear medicine. (A) Artificial intelligence is used in the projection domain to obtain more continuous sinogram data or to complete incomplete sinogram data. B) PET/SPECT images are produced directly from sinogram data using AI technology. (C) AI technology is used to create PET/SPECT images by directly enhancing the back-projection data. (D) Iterative reconstruction methods mixed with AI technologies. SPECT stands for single photon emission computed tomography, and PET is for positron emission tomography.

a DL technique is suggested that uses an encoder-decoder residual deep network with concatenate skip connections to solve this problem. The proposed method can produce better results than the state-of-the-art methods and reconstruct images with comparable quality using just 0.5% of the original regular dose, according to the analysis of ultra-low-dose clinical data. Similarly, Xiang et al. (2017) proposed using a CNN to predict full-dose PET images from PET images taken at 1/10th of a full dose [74]. The ROI statistics in the estimated images are generally on par with those in the actual full-dose images. In order to simulate a low-dose acquisition while still using the entire set of MR data, Chen et al. (2019) used the amyloid tracer Neuraceq from simultaneously acquired PET/MR imaging modalities to analyze one-hundredth of the acquired PET data scans, which is roughly the radiation exposure equivalent of a transcontinental flight. Following that, the experimental PET/MR was used as the reference standard for ML methods to predict the full-dose PET image. The experimentally acquired full-dose image was found to be satisfactorily reproduced by the simulated full-dose PET image [76]. In the study of Xiang et al. (2017) a DL architecture is seen to estimate the high-quality standard-dose PET (SPET) image from the combination of the low-quality low-dose PET (LPET) image and the accompanying T1-weighted acquisition from MRI. A comparison of this proposed method to state-of-the-art methods using validations on real PET/MRI data from the human brain demonstrates that it can provide competitive estimation quality of the PET images. As an example, this method estimates an entire SPET image in about 2 seconds as opposed to the state-of-the-art method's 16 minutes, demonstrating how effective it is for testing on new subjects. The aforementioned outcomes show how this method can be used in actual clinical applications [77]. In the same context, Wang et al. (2021) managed to construct a novel technique for separating high-quality full-dose PET images from low-dose ones based on 3D conditional GAN (3D c-GAN). In GAN, a discriminator network and a generator network are simultaneously trained with the intention of outperforming the other. In the proposed 3D c-GAN, which are similar to GAN, the model is conditioned on an input low-dose PET image and produces a corresponding output full-dose PET image. Experimental results demonstrate that our proposed 3D c-GAN method outperforms the benchmark methods and achieves significantly better performance than the state-of-the-art methods in both qualitative and quantitative measures [78]. In another study, Wang et al. (2021) recently demonstrated that the use of AI has the potential to lower the ^{18}F-FDG dosage to a 1/8 dose equivalent (0.18MBq/kg) while still producing interpretable images. Standardized uptake value (SUV) was untouched [75]. Another review negotiating the low-dose images is [11], in which a shallow ANN is developed that served as a learning-based denoising scheme using synaptic vesicle glycoprotein 2A radiotracer and image patches from 5 individuals' PET scans as the sample data. UCB-J. The authors processed 3-D image patches from reduced-count PET images using a MAP reconstruction algorithm as a learning-based denoising scheme, resulting in simulated full-count reconstruction image patches from the reduced-count data. Closing the section on lose dose imaging, it is worth mentioning the fact that recent papers refer to the potential of AI to forecast the post-therapy dosimetry of radiopharmaceuticals on an organ or voxel level. The complex relationship between the patient data collected prior to treatment and the radiation dose distribution received following treatment has been uncovered by the development of GAN, which may now be used to forecast the voxel-wise dose distribution for treatment planning. The training of an AI dosimetry prediction model also needs precise dose estimation. To replace Monte-Carlo simulation for voxel-wise dosimetry estimation, DL techniques have been developed [79, 80]. To improve dosimetry estimation from SPECT or PET measurements, preliminary results show that these methods are computationally effective when taking into account individual tissue density distributions as well as the heterogeneity of the radiopharmaceutical concentration. The low-dose imaging network structure is widely shown in Figure 5.

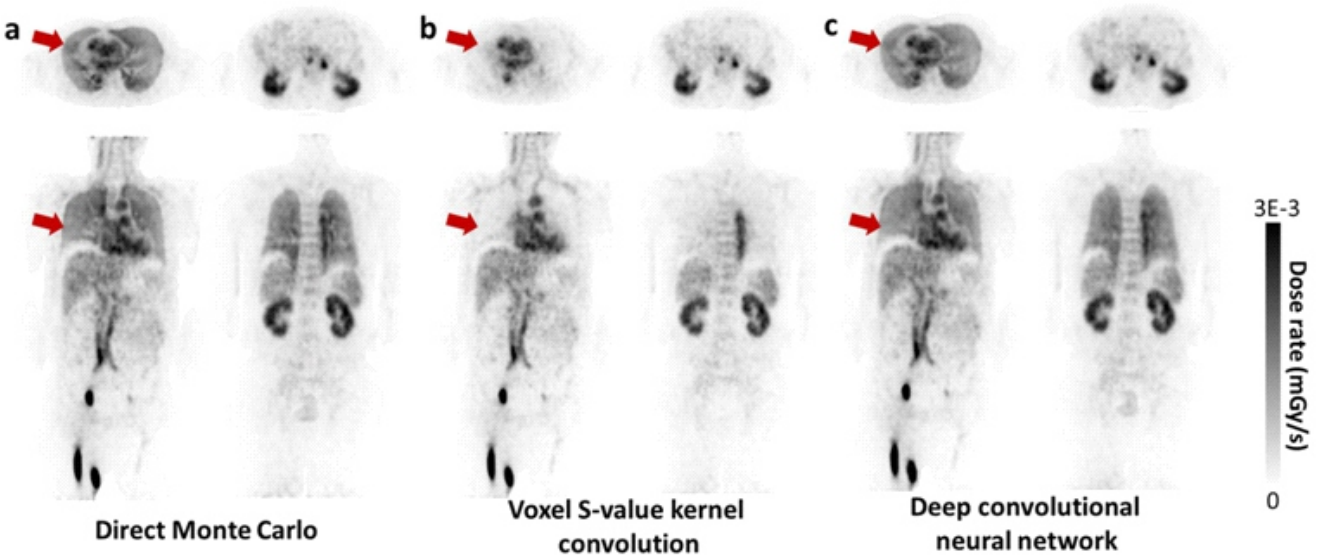

Figure 4. Dose rate maps estimated by (a) direct Monte Carlo, (b) VSV kernel convolution, and (c) deep convolutional neural network.

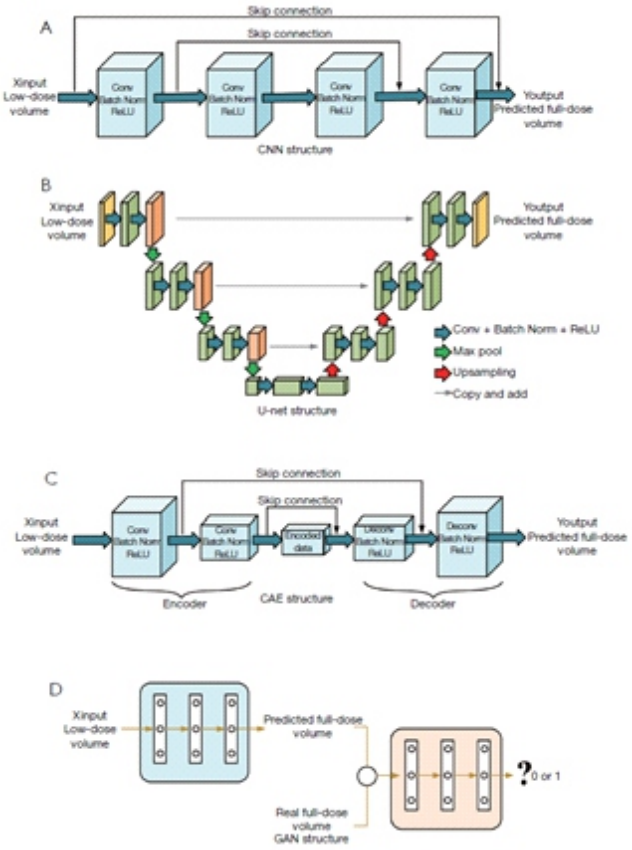

Figure 5. Low-dose imaging network structure. (A) The CNN structure here was essentially a low-pass filter, and the purpose of convolution was to extract useful features from the input. (B) At each stage of the U-net, two overlapping convolutional layers are designed to provide a deeper network. (C) For CAE, to ensure that the network output was the same size, a special design of padding and stride is essential. (D) For GAN, the generator network is used to create a full-dose image, and the discriminator network is used to distinguish predicted full-dose images and actual full-dose images. CNN, convolutional neural network; CAE, convolutional autoencoder; GAN, generative adversarial network.

In conclusion, the implementation of AI in NM Physics and Imaging is now a reality, and its existing applications are sufficient to demonstrate its utilization, both theoretically and, more importantly, practically. While the full potential of AI in this field is not yet fully understood, the first steps towards realizing it have already been taken. Despite its imperfections, there is no denying that AI will undoubtedly play a significant role in the future of healthcare.

Bibliography

1. Tang A, Tam R, Cadrin-Chênevert A et al. Canadian association of radiologists white paper on artificial intelligence in radiology. *Can Assoc Radiol J* 2018; 69(2): 120-35.
2. McBee MP, Awan OA, Colucci AT et al. Deep learning in radiology. *Academic Radiology* 2018; 25(11): 1472-80.
3. Langlotz CP, Allen B, Erickson BJ et al. A roadmap for foundational research on artificial intelligence in medical imaging: from the 2018 nih/rsna/acr/the academy workshop. *Radiology* 2019; 291(3): 781-91.
4. Decuyper M, Maebe J, Van Holen R, Vandenberghe S. Artificial intelligence with deep learning in nuclear medicine and radiology. *EJNMMI Phys* 2021; 8(1): 81.
5. Lundervold AS, Lundervold A. An overview of deep learning in medical imaging focusing on MRI. *Zeitschrift für Medizinische Physik* 2019; 29(2): 102-27.
6. Chartrand G, Cheng PM, Vorontsov E et al. Deep learning: a primer for radiologists. *RadioGraphics* 2017; 37(7): 2113-31.
7. Castiglioni I, Rundo L, Codari M et al. AI applications to medical images: From machine learning to deep learning. *Physica Medica* 2021; 83: 9-24.
8. Machine Learning. Available from: https://www.ibm.com/cloud/Learn/machine-learning.
9. Schulz MA, Yeo BTT, Vogelstein JT et al. Different scaling of linear models and deep learning in UKBiobank brain images versus machine-learning datasets. *Nat Commun* 2020; 11(1): 4238.
10. Uribe CF, Mathotaarachchi S, Gaudet V et al. Machine learning in nuclear medicine: part 1- introduction. *J Nucl Med* 2019; 60(4): 451-58.
11. Duffy IR, Boyle AJ, Vasdev N. Improving PET imaging acquisition and analysis with machine learning: a narrative review with focus on Alzheimer's disease and oncology. *Mol Imaging* 2019; 18: 153601211986907.
12. Magesh PR, Myloth RD, Tom RJ. An explainable machine learning model for early detection of parkinson's disease using lime on datscan imagery. *Computers in Biology and Medicine* 2020; 126: 104041.
13. Martin-Isla C, Campello VM, Izquierdo C et al. Image-based cardiac diagnosis with machine learning: a review. *Front Cardiovasc Med* 2020; 7: 1.
14. Toyama Y, Hotta M, Motoi et al. Prognostic value of ^{18}F-FDG-PET radiomics with machine learning in pancreatic cancer. *Sci Rep* 2020; 10(1): 17024.
15. Tang J, Yang B, Adams MP et al. Artificial neural network–based prediction of outcome in parkinson's disease patients using datscan SPECT imaging features. *Mol Imaging Biol* 2019; 21(6): 1165-73.
16. Moazemi S, Khurshid Z, Erle A et al. Machine learning facilitates hotspot classification in PSMA PET/CT with nuclear medicine specialist accuracy. *Diagnostics* 2020; 10(9): 622.
17. Huang G, Lin C, Cai Y et al. Multiclass machine learning classification of functional brain images for Parkinson's disease stage prediction. *Stat*

Anal Data Min: The ASA Data Sci Journal 2020; 13(5): 508-23.
18. Kaplan Berkaya S, Ak Sivrikoz I, Gunal S. Classification models for SPECT myocardial perfusion imaging. *Comp Biol Med* 2020; 123:103893.
19. Wang T, Lei Y, Fu Y et al. Machine learning in quantitative PET: A review of attenuation correction and low-count image reconstruction methods. *Physica Medica* 2020; 76: 294-306.
20. Zhang T, Shi M. Multi-modal neuroimaging feature fusion for diagnosis of Alzheimer's disease. *J Neurosci Methods* 2020; 341: 108795.
21. Papandrianos N, Papageorgiou E, Anagnostis A, Feleki A. A deep-learning approach for diagnosis of metastatic breast cancer in bones from whole-body scans. *Applied Sciences* 2020; 10(3): 997.
22. Liu Y, Xu Y, Meng X et al. A study on the auxiliary diagnosis of thyroid disease images based on multiple dimensional deep learning algorithms. *CMIR* 2020; 16(3): 199-205.
23. Hu Z, Li Y, Zou S et al. Obtaining PET/CT images from non-attenuation corrected PET images in a single PET system using Wasserstein generative adversarial networks. *Phys Med Biol* 2020; 65(21): 215010.
24. Xiang H, Lim H, Fessler JA, Dewaraja YK. A deep neural network for fast and accurate scatter estimation in quantitative SPECT/CT under challenging scatter conditions. *Eur J Nucl Med Mol Imaging* 2020; 47(13): 2956-67.
25. Reader AJ, Corda G, Mehranian A et al. Deep learning for pet image reconstruction. *IEEE Trans Radiat Plasma Med Sci* 2021; 5(1): 1-25.
26. Johnson A, Grumbling E. *Implications of Artificial Intelligence for Cybersecurity: Proceedings of a Workshop*. The National Academies Press; 2019.
27. Bal A, Banerjee M, Chaki R, Sharma P. An efficient method for PET image denoising by combining multi-scale transform and non-local means. *Multimed Tools Appl* 2020; 79(39-40): 29087-120.
28. Ramon AJ, Yang Y, Pretorius PH et al. Improving diagnostic accuracy in low-dose spect myocardial perfusion imaging with convolutional denoising networks. *IEEE Trans Med Imaging* 2020; 39(9): 2893-903.
29. Blanc-Durand P, Jégou S, Kanoun S et al. Fully automatic segmentation of diffuse large B cell lymphoma lesions on 3D ^{18}F-FDG-PET/CT for total metabolic tumour volume prediction using a convolutional neural network. *Eur J Nucl Med Mol Imaging* 2021; 48(5): 1362-70.
30. Wolterink JM. Left ventricle segmentation in the era of deep learning. *J Nucl Cardiol* 2020; 27(3): 988-991.
31. Sethi M, Ahuja S, Singh S et al. An intelligent framework for Alzheimer's disease classification using efficient net transfer learning model. In: *2022 International Conference on Emerging Smart Computing and Informatics (ESCI)* IEEE; 2022:1-4.
32. Hsu SY, Yeh LR, Chen TB et al. Classification of the multiple stages of parkinson's disease by a deep convolution neural network based on ^{99m}Tc-trodat-1 spect images. *Molecules* 2020; 25(20): 4792.
33. Liew C. The future of radiology augmented with Artificial Intelligence: A strategy for success. *Eur J Radiol* 2018; 102:152-6.
34. Gorospe-Sarasúa L, Muñoz-Olmedo JM, Sendra-Portero F, De Luis-García R. Challenges of Radiology education in the era of artificial intelligence. *Radiología (English Edition)* 2022; 64(1): 54-9.
35. Thrall JH, Li X, Li Q et al. Artificial intelligence and machine learning in radiology: opportunities, challenges, pitfalls, and criteria for success. *J Ame Coll Radiol* 2018; 15(3): 504-8.
36. Visvikis D, Lambin P, Beuschau Mauridsen K et al. Application of artificial intelligence in nuclear medicine and molecular imaging: a review of current status and future perspectives for clinical translation. *Eur J Nucl Med Mol Imaging* 2022; 49(13): 4452-63.
37. Nensa F, Demircioglu A, Rischpler C. Artificial intelligence in nuclear medicine. *J Nucl Med* 2019; 60 (Supplement 2): 29S-37S.
38. Lee JS. A review of deep-learning-based approaches for attenuation correction in positron emission tomography. *IEEE Trans Radiat Plasma Med Sci* 2021; 5(2): 160-84.
39. Dong X, Lei Y, Wang T et al. Deep learning-based attenuation correction in the absence of structural information for whole-body positron emission tomography imaging. *Phys Med Biol* 2020; 65(5): 055011.
40. Jang H, Liu F, Zhao G et al. Technical Note: Deep learning based MRAC using rapid ultrashort echo time imaging. *Med Phys* 2018; 45(8): 3697-3704.
41. Hwang D, Kang SK, Kim KY et al. Generation of pet attenuation map for whole-body time-of-flight ^{18}F-FDG PET/MRI using a deep neural network trained with simultaneously reconstructed activity and attenuation maps. *J Nucl Med* 2019; 60(8): 1183-9.
42. Liu F, Jang H, Kijowski R et al. A deep lear-ning approach for ^{18}F-FDG PET attenuation correction. *EJNMMI Phys* 2018; 5(1): 24.
43. Ladefoged CN, Marner L, Hindsholm A et al. Deep learning based attenuation correction of PET/MRI in pediatric brain tumor patients: evaluation in a clinical setting. *Front Neurosci* 2019; 12: 1005.
44. Weng W, Zhu X. Inet: convolutional networks for biomedical image segmentation. *IEEE Access* 2021; 9: 16591-603.
45. Cheng Z, Wen J, Huang G, Yan J. Applications of artificial intelligence in nuclear medicine image generation. *Quant Imaging Med Surg* 2021; 11(6): 2792-822.
46. Shi L, Onofrey JA, Liu H et al. Deep learning-based attenuation map generation for myocardial perfusion *SPECT. Eur J Nucl Med Mol Imaging* 2020; 47(10): 2383-95.
47. Dong X, Wang T, Lei Y et al. Synthetic CT generation from non-attenuation corrected PET images for whole-body PET imaging. *Phys Med Biol* 2019; 64(21): 215016.
48. Gong K, Yang J, Larson PEZ et al. Mr-based attenuation correction for brain pet using 3-d cycle-consistent adversarial network. *IEEE Trans Radiat Plasma Med Sci* 2021; 5(2): 185-92.
49. Armanious K, Hepp T, Küstner T et al. Independent attenuation correction of whole body ^{18}F-FDG-PET using a deep learning approach with Generative Adversarial Networks. *EJNMMI Res* 2020; 10(1): 53.
50. Yang J, Park D, Gullberg GT, Seo Y. Joint correction of attenuation and scatter in image space using deep convolutional neural networks for dedicated brain ^{18}F-FDG PET. *Phys Med Biol* 2019; 64(7): 075019.
51. Shiri I, Arabi H, Geramifar P et al. Deep-JASC: joint attenuation and scatter correction in whole-body ^{18}F-FDG PET using a deep residual network. *Eur J Nucl Med Mol Imaging* 2020; 47(11): 2533-48.
52. Berker Y, Maier J, Kachelries M. Deep scatter estimation in pet: fast scatter correction using a convolutional neural network. In: *2018 IEEE Nuclear Science Symposium and Medical Imaging Conference Proceedings (NSS/MIC)* IEEE; 2018: 1-5.
53. Qian H, Rui X, Ahn S. Deep learning models for pet scatter estimations. In: *2017 IEEE Nuclear Science Symposium and Medical Imaging Conference (NSS/MIC)* IEEE; 2017: 1-5.
54. Zatcepin A, Pizzichemi M, Polesel A et al. Improving depth-of-interaction resolution in pixellated PET detectors using neural networks. *Phys Med Biol* 2020; 65(17): 175017.
55. Michaud JB, Tetrault MA, Beaudoin JF et al. Sensitivity increase through a neural network method for LOR recovery of ICS triple coincidences in high-resolution pixelated- detectors pet scanners. *IEEE Trans Nucl Sci* 2015; 62(1): 82-94.
56. Johnstone IM, Silverman BW. Speed of estimation in positron emission tomography and related inverse problems. *Ann Statist* 1990; 18(1), 251-80.
57. Bruyndonckx P, Leonard S, Tavernier S et al. Neural network-based position estimators for PET detectors using monolithic LSO blocks. *IEEE Trans Nucl Sci* 2004; 51(5): 2520-25.
58. Tavernier S, Bruyndonckx P, Leonard S, Devroede O. A high-resolution PET detector based on continuous scintillators. *Nuclear Instruments and Methods in Physics Research Section A: Accelerators, Spectrometers, Detectors and Associated Equipment* 2005; 537 (1-2): 321-25.
59. Bruyndonckx P, Lemaitre C, Van Der Laan DJ et al. Evaluation of machine learning algorithms for localization of photons in undivided scintillator blocks for pet detectors. *IEEE Trans Nucl Sci* 2008; 55(3): 918-24.
60. Wang Y, Zhu W, Cheng X, Li D. 3D position estimation using an artificial neural network for a continuous scintillator PET detector. *Phys Med Biol* 2013; 58(5): 1375-90.
61. Iborra A, González AJ, González-Montoro A et al. Ensemble of neural networks for 3D position estimation in monolithic PET detectors. *Phys Med Biol* 2019; 64(19): 195010.
62. Decuyper M, Stockhoff M, Vandenberghe S, Van Holen R. Artificial neural networks for positioning of gamma interactions in monolithic PET detectors. *Phys Med Biol* 2021; 66(7): 075001.
63. Berg E, Cherry SR. Using convolutional neural networks to estimate time-of-flight from PET detector waveforms. *Phys Med Biol* 2018; 63(2): 02LT01. doi:10.1088/1361-6560/aa9dc5.
64. Ravishankar S, Ye JC, Fessler JA. Image reconstruction: from sparsity to data-adaptive methods and machine learning. *Proc IEEE* 2020; 108(1): 86-109.
65. Häggström I, Schmidtlein CR, Campanella G, Fuchs TJ. DeepPET: A deep encoder-decoder network for directly solving the PET image reconstruction inverse problem. *Medical Image Analysis* 2019; 54: 253-62.

66. Kandarpa VSS, Bousse A, Benoit D, Visvikis D. Dug-recon: a framework for direct image reconstruction using convolutional generative networks. *IEEE Trans Radiat Plasma Med Sci* 2021; 5(1): 44-53.
67. Zhu B, Liu JZ, Cauley SF et al. Image reconstruction by domain-transform manifold learning. *Nature* 2018; 555(7697): 487-92.
68. Yang B, Ying L, Tang J. Artificial neural network enhanced bayesian pet image reconstruction. *IEEE Trans Med Imaging* 2018; 37(6): 1297-309.
69. Hong X, Zan Y, Weng F et al. Enhancing the image quality via transferred deep residual learning of coarse pet sinograms. *IEEE Trans Med Imaging* 2018; 37(10): 2322-32.
70. Kim K, Wu D, Gong K et al. Penalized pet reconstruction using deep learning prior and local linear fitting. *IEEE Trans Med Imaging* 2018; 37(6): 1478-87.
71. Liu CC, Qi J. Higher SNR PET image prediction using a deep learning model and MRI image. *Phys Med Biol* 2019; 64(11): 115004.
72. Gong K, Guan J, Liu CC, Qi J. Pet image denoising using a deep neural network through fine tuning. *IEEE Trans Radiat Plasma Med Sci* 2019; 3(2): 153-61.
73. Xu J, Gong E, Pauly J, Zaharchuk G. 200x low-dose pet reconstruction using deep learning. Published online December 11, 2017. Accessed March 1, 2023. http://arxiv.org/abs/1712.04119.
74. Kaplan S, Zhu YM. Full-dose pet image estimation from low-dose pet image using deep learning: a pilot study. *J Digit Imaging* 2019; 32(5): 773-8.
75. Wang YR, Baratto L, Hawk KE et al. Artificial intelligence enables whole-body positron emission tomography scans with minimal radiation exposure. *Eur J Nucl Med Mol Imaging* 2021; 48(9): 2771-60.
76. Chen KT, Gong E, De Carvalho Macruz FB et al. Ultra–low-dose ^{18}F-florbetaben amyloid pet imaging using deep learning with multi-contrast mri inputs. *Radiology* 2019; 290(3): 649-56.
77. Xiang L, Qiao Y, Nie D et al. Deep auto-context convolutional neural networks for standard-dose PET image estimation from low-dose PET/MRI. *Neurocomputing* 2017; 267: 406-16.
78. Wang Y, Yu B, Wang L et al. 3D conditional generative adversarial networks for high-quality PET image estimation at low dose. *Neuro Image* 2018; 174: 550-62.
79. Shi K, Dong C, Gafita A et al. Artificial neural network for prediction of post-therapy dosimetry for ^{177}Lu-PSMA I&T therapy. *Nuklearmedizin* 2019; 58: 118.
80. Lee MS, Hwang D, Kim JH, Lee JS. Deep-dose: a voxel dose estimation method using deep convolutional neural network for personalized internal dosimetry. *Sci Rep* 2019; 9(1): 10308.